Available online at www.sciencedirect.com

ScienceDirect

Energy Procedia 63 (2014) 2821 – 2830

Energy Procedia

GHGT-12

# The Green River natural analogue as a field laboratory to study the long-term fate of $CO_2$ in the subsurface

A. Busch[a]*, N. Kampman[b,c], S.J. Hangx[a,d], J. Snippe[a], M. Bickle[e], P. Bertier[f], H. Chapman[e], C.J. Spiers[d], R. Pijnenburg[d], J. Samuelson[d], J. P. Evans[g], A. Maskell[e], J. Nicholl[e], V. Pipich[h], Z. Di[h], G. Rother[i], M. Schaller[j]

[a]*Shell Global Solutions International, Rijswijk, NL*
[b]*Lancaster Environment Centre, Lancaster University, UK*
[c]*British Geological Survey, Keyworth, Nottingham, UK*
[d]*High Pressure and Temperature Laboratory, Utrecht University, NL*
[e]*Department of Earth Sciences, University of Cambridge, UK*
[f]*RWTH Aachen University, Clay and Interface Mineralogy, GER*
[g]*Department of Geology, Utah State University, Logan, UT, USA*
[h]*Jülich Centre for Neutron Science JCNS, Garchig, GER*
[i]*Chemical Sciences Division, Oak Ridge National Laboratory, Oak Ridge, USA*
[j]*Department of Earth and Planetary Sciences, Rutgers University, USA*

**Abstract**

Understanding the long-term response of $CO_2$ injected into porous reservoirs is one of the most important aspects to demonstrate safe and permanent storage. In order to provide quantitative constraints on the long-term impacts of $CO_2$-charged fluids on the integrity of reservoir-caprock systems we recovered some 300m of core from a scientific drill hole through a natural $CO_2$ reservoir, near Green River, Utah. We obtained geomechanical, mineralogical, geochemical, petrophysical and mineralogical laboratory data along the entire length of the core and from non $CO_2$-charged control samples. Furthermore, we performed more detailed studies through portions of low permeability layers in direct contact with $CO_2$-charged layers. This was done to constrain the nature and penetration depths of $CO_2$-promoted fluid-mineral reaction fronts. The major reactions identified include the dissolution of diagenetic dolomite cements and hematite grain coatings, and the precipitation of ankerite and pyrite and have been used as input for geochemical 1D reactive transport modelling, to constrain the magnitude and velocity of the mineral-fluid reaction front.

In addition, we compared geomechanical data from the $CO_2$-exposed core and related unreacted control samples to assess the mechanical stability of reservoir and seal rocks in a $CO_2$ storage complex following mineral dissolution and precipitation for thousands of years. The obtained mechanical parameters were coupled to mineralogy and porosity. Key aim of this work was to

* Corresponding author. Tel.: +31(0)70-447-5899
*E-mail address:* andreas.busch@shell.com


Peer-review under responsibility of the Organizing Committee of GHGT-12
doi:10.1016/j.egypro.2014.11.304

better quantify the effect of long-term chemical $CO_2$/brine/rock interactions on the mechanical strength and elastic properties of the studied formations.


Peer-review under responsibility of the Organizing Committee of GHGT-12

*Keywords:* Natural $CO_2$ analogue, reaction profile, $CO_2$-water-rock interaction, Green River

## Introduction and Background

Understanding the geochemical behaviour of carbon dioxide stored in geological reservoirs over a range of time-scales is crucial for quantifying the risk of leakage and the geochemical evolution of the stored $CO_2$ through the life of an individual storage site (see review in Kampman et al. [1]). $CO_2$ dissolution in brine will tend to stabilize the $CO_2$ in storage reservoirs (e.g. [2]) and reactions between $CO_2$-charged brines and reservoir minerals might either enhance the long-term storage security by precipitation of carbonate minerals or facilitate leakage through mineral dissolution and corrosion of caprocks and fault seals (e.g. [3]). A further concern is that migration and intrusion of $CO_2$ will drive acidification of potable groundwater which may mobilize potentially toxic metals.

There are various ways for buoyant supercritical $CO_2$ to leak from a storage reservoir, either by natural (e.g. permeable faults, natural fractures, pore system of sealing rocks, lateral discontinuity) or by artificial pathways (e.g. wellbores, activated faults/fractures). On the one hand a deep understanding of the fluid-fluid and fluid-rock reactions that may retard the migration of $CO_2$ from deep storage sites to the surface is of critical importance for demonstrating the retentive capacity of the geological overburden, above deep storage reservoirs. On the other hand understanding the changes to rock mechanical properties related to these fluid-rock reactions are needed from basic principles to eliminate the risk of rock weakening, followed by mechanical breaching of the seal or wellbore issues. While monitoring systems in the wellbore, at the land surface or sea floor are well advanced and the density of point measurements is mainly a matter of accessibility and cost, we are still lacking basic concepts and mechanisms of the long term fate of $CO_2$ in the subsurface. Laboratory studies have the potential to indicate $CO_2$/water/rock reaction patterns for time scales in the order of weeks or months (in rare cases even a few years), hence cover far from equilibrium conditions; the long term behavior of up to 10,000 years (as requested by many regulators) can however only be covered by a thorough understanding of natural systems.

For the purpose of investigating the effects of carbonated brine on flow and reactions in caprocks and the changes in mechanical properties of shales and sandstones, we performed a coring and downhole fluid sampling campaign of a natural $CO_2$ system at Green River, Utah. Details of this campaign have been summarized earlier [4, 5] and we here only focus on some important aspects to set the scene.

The ~322 m deep vertical hole (CO2W55) was drilled in July 2012, penetrating a stacked sequence of $CO_2$-charged Jurassic sandstone reservoirs (Entrada and Navajo Fms.) and their intervening caprocks (Carmel Fm.). These shallow reservoirs are filled through a normal fault system (Little Grand Wash fault, LGW) through which $CO_2$ and $CO_2$-charged fluids migrate from deep supercritical $CO_2$ reservoirs at depth within the basin [4-7]. We were able to obtain full core recovery and pressurized fluids (water and gas) from several depths within the Navajo sandstone (for pH and $CO_2$ contents) as well as de-pressurized surface samples from various depths within Entrada and Navajo. Rocks and fluids are now studied for many purposes, including reservoir behavior when charged with $CO_2$, caprock reactions and implications on flow and porosity, mineral carbonation potential in the reservoir or rock mechanical effects due to changes in rock properties. We used many different analytical and experimental methods, like X-ray diffraction (XRD), X-ray fluorescence (XRF), element and isotope geochemistry, low-pressure $N_2$ sorption to determine surface area and pore volume, small and ultra-small angle neutron scattering (USANS, SANS) to determine porosity and surface area, conventional porosimetry and permeameter tests on plugs, microprobe, optical and electron microscopy as well as rock mechanical uniaxial and triaxial plug testing to determine rock strength and potential fault behavior.

In addition PHREEQC3 [8] as standalone or the coupled MoReS-PHREEQC (MoReS being the Shell in-house reservoir simulator [9]) geochemical and reactive transport modeling codes respectively have been used to reproduce reaction features found within this natural $CO_2$ analogue.

The detailed focus of this article is two-fold: (1) we describe a reaction profile from a high permeable layer, charged with $CO_2$-rich fluids, into a low permeability, clay rich layer within the Entrada sandstone. This reaction profile is macroscopically visible by a relatively sharp bleaching front into the red clayey siltstone. Methods used here are stable isotope studies, XRD, XRF, (U)SANS, and N2-BET and will be described in detail below; and (2) we compared mechanical strength and elasticity parameters of Navajo sandstone from the drill hole and related non-reacted formations to potentially observe differences and to relate those to porosity and mineralogy.

## Reaction profile along low permeability siltstone layer

### *Mineralogy, petrophysics and geochemistry*

We sampled a silty claystone section of Entrada from the location given in Figure 1, showing distinct bleaching features and covering a thickness of 10.4 cm. This section was split into 26 single samples with a sampling interval of 4 mm. We determined mineralogy, chemistry and S, O, and C stable isotopes on each of these samples. Specific surface area and porosity using low pressure $N_2$ sorption and (U)SANS were determined on a selection of these samples only.

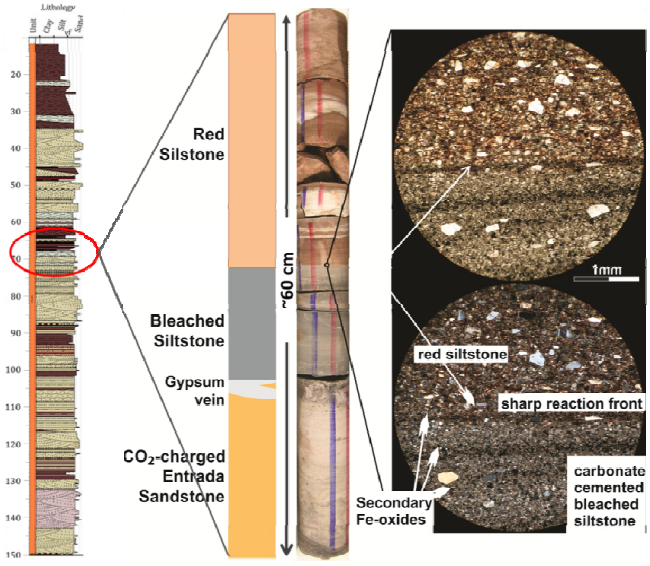


Figure 1: Entrada formation from surface to top Carmel Fm with $CO_2$-charged sandstone layer, overlain by a low permeability clayey siltstone showing bleaching and $CO_2$ reaction features. A sharp contact between bleached and unbleached is observed.

X-ray diffraction (XRD) measurements to determine mineralogy has been performed at RWTH Aachen University as described in e.g. [10]. Quantitative phase analysis was performed by Rietveld refinement using BGMN software, with customized clay mineral structure models [11]. The precision of these measurements, from repetitions, is better than 0.1 wt-% for phases of which the content is above 2%. The accuracy is difficult to determine because of the lack of high purity clay mineral reference materials, but is estimated to be better than 10% (relative).

Major elemental compositions were determined by energy dispersive X-ray fluorescence spectrometry (XRF) at Open University with a Spectro XLab2000 spectrometer, equipped with a Pd-tube and Co, Ti and Al as secondary targets. Precisions and accuracy, as determined from repeated measurements on standards, are better than 0.5 wt-%.

For specific surface area, micropore volume and pore radius distribution, low-pressure $N_2$ gas adsorption isotherms were measured at 77.3K, by means of the static-volumetric method, using a Micromeritics Gemini VII 2390t device. Adsorption/desorption was measured at 71 relative pressure steps between 0.001 and 0.995. The multipoint BET-method was applied to calculate surface areas, conform to the ISO 9277:2010 standard. A cross-sectional area of the nitrogen molecule of 0.162 $nm^2$ was used. Differential mesopore volume distributions were calculated from the desorption branch of the isotherms using the Barret-Joyner-Halenda theory, using the Harkins-Jura thickness equation with Faas correction (for $P/P_0$ >0.35), conform to the DIN 66134 norm. Gurvich total pore volume was determined from adsorption at a relative pressure of 0.995.

Small angle Neutron scattering (SANS) experiments were carried out using the instrument KWS-1 (SANS) and KWS-3 (USANS) operated by the Jülich Center for Neutron Science (JCNS) at Heinz-Meier-Leibnitz Zentrum (MLZ) in Garching, Germany. Entrada samples were cut and polished to a thickness of 200 microns and fixed on quartz glass for measurements. Data were collected at wavelengths of $\lambda$ = 6.9 Å with a wavelength distribution of the velocity selector $\Delta\lambda/\lambda$=0.10 (full width at half-maximum). Measurements were performed at sample-to-detector distances of 19.7 m, 7.7 m and 1.7 m, therefore covering a wide q-range of 0.002 – 0.26 $Å^{-1}$. The detector was a 6Li glass scintillation detector with an active area of 60×60 $cm^2$. Instrument data analysis and background subtraction was carried out using the QtiKWS software provided by JCNS [12]. In order to cover the broader length scale of the network structure, USANS experiments were carried out at the KWS-3 diffractometer using a parabolic mirror as an optical element, and covering the smaller Q range from 0.01 to 0.2 $Å^{-1}$. Data interpretation (calculation of porosity and specific surface area) was performed using the PRINSAS software [13].

*Description and modeling of siltstone reaction profile*

The siltstone layer consists on average of equally 39 wt.% quartz and illite with some minor contributions of dolomite, K-feldspar, pyrite, hematite, albite and some trace minerals. The layer is partially bleached from its original reddish color, caused by up to 2 m-% hematite (Figure 1) with a sharp contact at about 67.66 m. This bleaching is assumed to be due to hematite reduction by a reducing agent such as $H_2S$. The iron mobilization from hematite dissolution caused pyrite to precipitate in the bleached section with two distinct peaks at about 67.675 and 67.69 m depth. Pyrite contents in the unbleached section were essentially zero. In the bleached part we also observe a gradual increase in dolomite contents from about 3 wt.% at the base (~67.74 m) to ~10 wt.% at the reaction front. In the unbleached section dolomite contents are constant at ~10-12 wt.%. Dissolution of dolomite in the bleached section is accompanied by reprecipitation of ankerite over existing dolomite grains, observed in SEM images. Similarly, CaO, MgO, and $Fe_2O_3$ contents in the unbleached are generally higher than in the bleached section

Porosity and specific surface area (SSA) for the two methods used ($N_2$-adsorption and SANS) are reasonably similar, despite some differences in accessibility for the two methods. There is a small difference in the overall magnitude of the porosity (3-4%) between reacted and unreacted intervals. $N_2$-adsorption data show no clear spatial trend while SANS data suggests a slight decrease in porosity with depth (from ~4.5 to 4%), which could be due to sedimentological features. SSA data for the two methods are similar with values of ~8-12 $m^2/g$ and are not considered to relate to any reaction patterns but rather to slight changes in the illite.

Fluid chemistry used for modeling was taken from Kampman et al. [4]. We further assumed some minor contribution of $H_2S$ as reductant causing the bleaching (hematite dissolution). From the chemical and mineralogical changes we infer the dissociation of $H_2S$ and $CO_2$ in brine and the subsequent reduction of hematite to form pyrite as well as dissolution of dolomite and reprecipitation of ankerite (Equ. 1-6):

$$H_2S \rightleftharpoons HS^- + H^+ \quad (1)$$

$$CO_2 + H_2O \rightleftharpoons H_2CO_3 \leftrightarrow HCO_3^- + H^+ \quad (2)$$

$$4Fe_2O_3 + H_2S + 14CO_2 + 6H_2O \rightleftharpoons 8Fe^{2+} + 14HCO_3^- + SO_4^{2-} \quad (3)$$

$$2HS^- + Fe^{2+} \rightleftharpoons FeS_2 + 2H^+ \quad (4)$$

$$CaMg(CO_3)_2 + 2H^+ \rightleftharpoons Ca^{2+} + Mg^{2+} + 2HCO_3^- \quad (5)$$

$$Ca^{2+} + 0.7Mg^{2+} + 0.3Fe^{2+} + 2HCO_3^- \rightleftharpoons Ca(Mg_{0.7}Fe_{0.3})(CO_3)_2 + 2H^+ \quad (6)$$

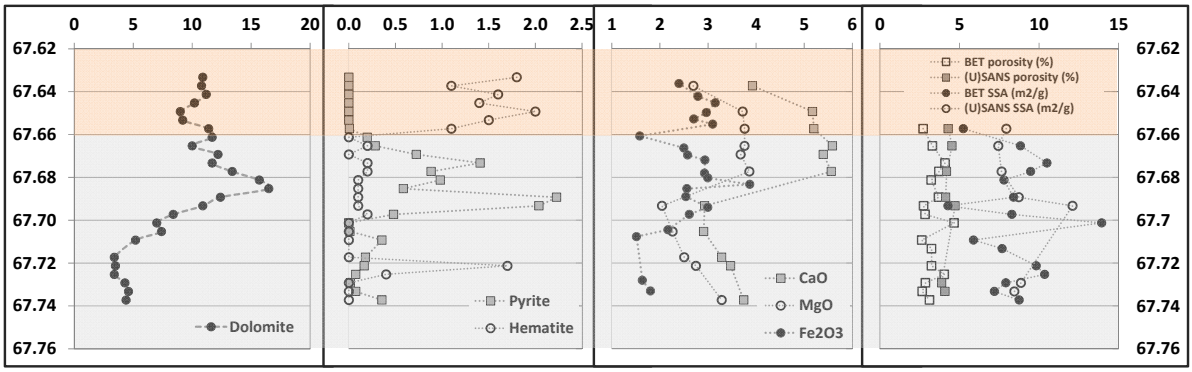


Figure 2: Reaction profile along a 10.4 cm thick low permeability layer of predominantly clayey siltstone. Reacted section is indicated in grey shading, non-reacted part in orange. Mineralogy (from XRD) and chemistry (from XRF) are in weight-%.

Fluid-mineral reactions inferred from changes in the caprock mineralogy and from petrological observations were modeled using PHREEQC. The reactive transport model comprises a 1D column of thirty cells, 1 cm in length, representing the intra-formational seal. Initial model parameters are summarized in Table 1. The initial modal mineralogy of the cells was based on a representative sample of unreacted siltstone from the Entrada Sandstone (Fig. 1). $CO_2$-saturated Na-Cl-$SO_4$ brine, with a composition determined by sampling of reservoir fluids from the Green River accumulation [4], was allowed to diffuse into the caprock cells over a 100kyr period, and the resulting change in mineralogy was recorded. The initial cell porosity (4%) was determined from BET analyses. An effective diffusivity was estimated from measured porosity and a representative tortuosity for siltstones, obtained from the literature. Results of the modeling attempt are provided in Figure 3 for five different time steps (1, 20, 45 and 90 kyrs as well as present day). Present day data refers to the measured data (cf. Figure 2). The reactive transport model was run as an 'instantaneous equilibrium model', without kinetic rate constants or reactive surface area data. The front propagation is controlled by initial mineral abundance, mineral solubility, secondary mineral precipitation and the effective diffusivity ($5x10^{-12}$ $m^2/s$) of species ($CO_2$+$HS^-$) driving the front forward. The model gives qualitatively good results and compares well between the 90 kyrs and the present day plot (Figure 3). The results suggest that the observed pattern of reactions developed over an ~90kyr period of reactive flow, which is in reasonable agreement with age constraints for an active $CO_2$-charge of the reservoir over the last 113 kyrs, based on U-series dating of travertine deposits along LGW [7]. The model predicts hematite dissolution and pyrite precipitation, as well as a slight dolomite increase just below the reaction front, followed by a decrease in these contents (dissolution) towards the base of the shale layer. Species mobilized by the dissolution of hematite and dolomite are reprecipitated on and behind the propagating fronts as ankerite, in agreement with petrological observations. The modeled peak in pyrite concentration is shifted by few cm towards the base of the layer but qualitatively matches. This mismatch might get resolved by introducing different pulses of $CO_2$/$H_2S$ into the sand layer below the shale package which is considered likely [6]. Other mineral phases like K-feldspar (5-10 wt.%) and illite (35-40 wt.%) are not plotted here, although they were modeled, since there is only a minor contribution of these minerals to the main reactions.

Table 1: Input parameters for geochemical modelling.

| Model Parameters | $CO_2$ Diffusivity | Porosity | Tortuosity | Effective Diffusivity | Initial Mineralogy (mol/L) | | |
|---|---|---|---|---|---|---|---|
| | | | | | Hematite | Dolomite | K-feldspar |
| Entrada Siltstone | $2x10^{-9}$ | 4% | 16 | $5x10^{-12}$ | 6.8 | 41.5 | 50.0 |

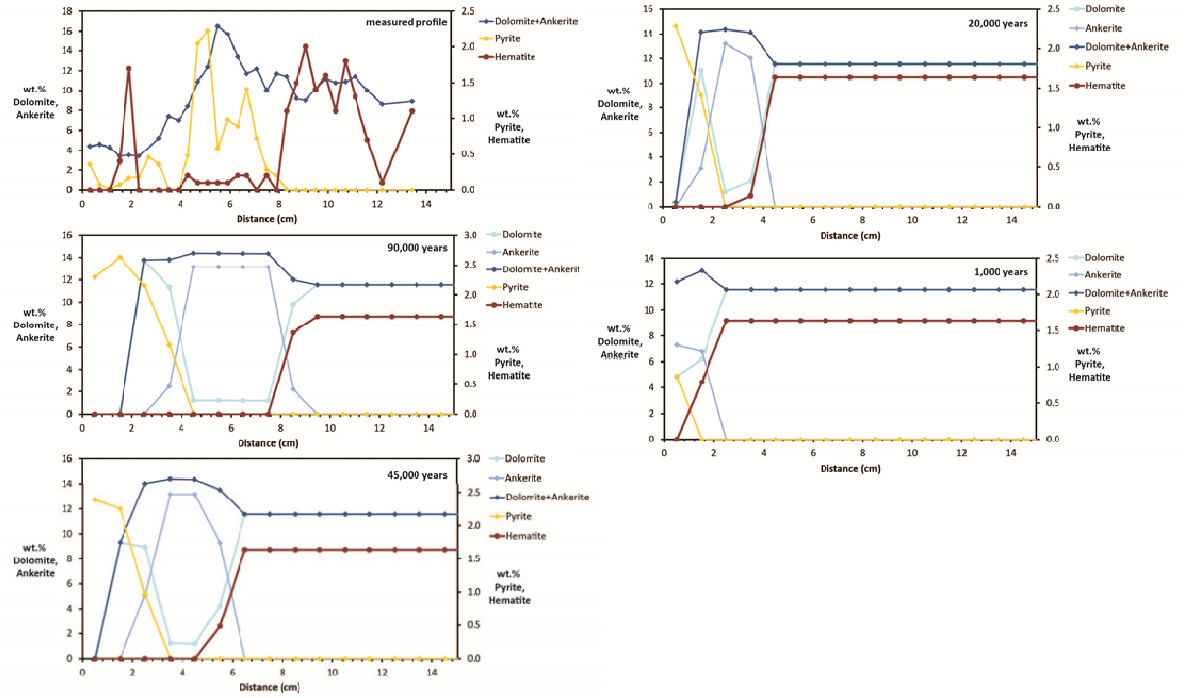


Figure 3: Modeled reactions along the siltstone layer for time scales of 1, 20, 45 and 90 kyears as well as present day (measured) profile. The base of the layer (at 0 cm) is the interface to a high permeability sandstone layer. $CO_2$ and $H_2S$ is introduced from the interface. Siltstone properties have been measured for all parameters over a length of 10.4 cm (Fig. 2) while the model studies a 15 cm thick profile.

## Chemical-mechanical coupling for the reservoir: impact of $CO_2$-exposure on mechanical parameters

In addition to the petrophysical and geochemical analysis of the rocks obtained from the Green River drilling site, we also investigated the mechanical properties of the reservoir and caprock. Mechanical experiments were performed on samples taken from the Navajo Sandstone formation, using a conventional triaxial testing apparatus, see Hangx et al. [14, 15] for a detailed description. Complementary tests were performed on material from the same stratigraphic unit, but unexposed to $CO_2$. All experiments were done at room temperature, at applied confining pressures $P_c$ in the range 5 to 65 MPa, under dry or wet (artificial reservoir brine, pore pressure $P_p$ = 15 MPa) conditions, at a strain rate of ~$10^{-5}$ $s^{-1}$. In this study, we take compressive stresses as positive. The principal compressive stresses are denoted $\sigma_i$, with $\sigma_1 > \sigma_2 = \sigma_3 = P_c$. Principal effective stresses are accordingly denoted $\sigma_i^{eff}$, and are defined as $\sigma_i^{eff} = \sigma_i - P_p$. From our stress-strain data, we defined peak differential stress $(\sigma_1 - \sigma_3)_{max}$ as the maximum stress supported by a given sample, where failure is indicated as the loss of strength of the rock beyond the peak, either via catastrophic brittle fracturing or more gradual strain softening. Apparent Young's Modulus values ($E_a$) are determined for the linear-elastic part of the stress-strain curves [16, 17].

We plotted our strength data in Mohr-Coulomb stress space, using conventional Mohr circles to describe the stress state during failure in compression, as shown in Figure 4. Overall, peak strength increases with confining pressure for all three materials, which is typical for high-porosity rocks, see e.g. [18]. As can be seen, the Navajo Sandstone obtained from the Green River drill hole (i.e. $CO_2$-exposed) is significantly stronger than its unreacted counterparts. Furthermore, material tested under dry conditions is generally stronger than under wet conditions (cf. dotted vs. solid circles in Figure 4).

By expressing our data in Mohr-Coulomb stress space, we obtained linear relationships, so-called failure envelopes, describing some of the key mechanical parameters of the different sandstones, i.e. cohesion ($S_0$) and the internal friction angle ($\Phi$). Such a relationship has the form:

$$\tau = S_0 + \mu(\sigma_n - P_p) \quad (5)$$

Where, $\tau$ is the maximum shear stress on the fault plane, $\mu$ is the internal friction coefficient ($\mu = \tan \Phi$) and $\sigma n$ is the stress normal to the fault plane. Using a best-fit method, the following three relationships were determined for each of the materials:

Green River ($CO_2$-exposed): $\tau = 12.464 + 1.2598\ (\sigma_n - P_p)$ ($R^2 = 0.93$) (6a)

Big Hole (unreacted): $\tau = 14.981 + 0.6876\ (\sigma_n - P_p)$ ($R^2 = 0.98$) (6b)

I-70 (unreacted): $\tau = 12.499 + 0.7984\ (\sigma_n - P_p)$ ($R^2 = 0.86$) (6c)

Given the derived cohesion and friction angle, the unconfined compressive strength (UCS) can be calculated, using $UCS = =(2S_0 \cos\Phi)/(1-\sin\Phi)$. UCS values for the Green River, Big Hole and I-70 Navajo Sandstones are 71, 57 and 52 MPa, respectively. When looking at the elastic properties (apparent Young's Modulus $E_a$) of the different materials, a trend similar to that for peak strength can be seen, displaying increasing E with confining pressure until steady values are reached at $P_c > 15$ MPa (Figure 5). Note that, we used $E_a$ because the elastic compaction of a rock always still contains some inelastic behavior.

In explaining these results, it should be noted that one of the most important petrophysical parameters controlling rock mechanical behaviour is porosity (e.g. see [18]). This influences the magnitude of stresses transmitted from grain to grain. The average porosity of the $CO_2$-exposed Green River Navajo Sandstone is ~12.5%, while those for the unreacted Big Hole and I-70 samples are systematically higher at ~20.3 and ~17.2%, respectively (see porosity values indicated in Figure 4). The lower porosity is most likely the main cause for the higher strength of the Green River material. Given the diagenetic history of the Navajo Sandstone, there are two main hypotheses for explaining the differences in rock porosity: 1) $CO_2$-related dolomite precipitation in the Green River sandstone, and 2) different depositional and burial depth histories, resulting in different porosities among the sample locations.

To test the former, we performed Thermo-Gravimetric Analysis (TGA) of the samples – see Figure 4, where the TGA data on dolomite wt-% are also indicated. Overall, there seems to be no clear correlation between the amount of dolomite present and rock strength, with some high porosity samples also containing several wt-% of dolomite. However, this is only true looking at the mechanical behaviour of the Navajo Sandstone formation as a whole. Detailed core scratch testing, performed on selected sections of the reservoir (Green River, $CO_2$-exposed), show that UCS is indeed correlated to dolomite (carbonate) content, as can be seen in Figure 6. Therefore, it is inferred that differences in depositional environment and burial history lie at the foundation of the differences in mechanical behaviour of the three materials on the reservoir (10-100 m-size) scale, though local variations in dolomite content affect mechanical properties on a smaller (cm-size) scale.

In addition to the geomechanical work done on the Navajo Sandstone, we are currently performing experiments on the Carmel caprock Formation, using a novel technique to measure the mechanical properties of low-permeability rocks. Though proof of concept has been achieved, preliminary results are not yet available.

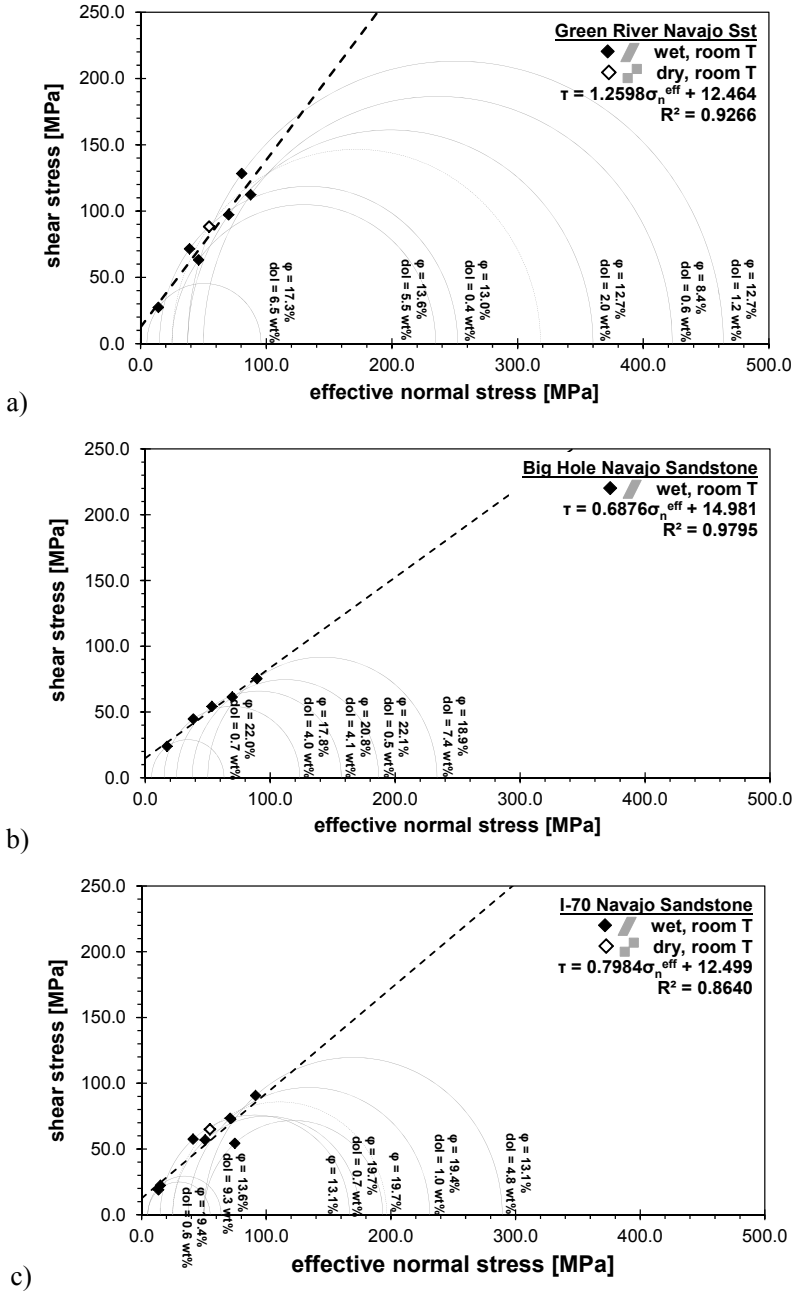


Figure 4. Mohr-Coulomb circles and failure envelopes for Navajo Sandstone, obtained from the three different sampling locations: a) Green River ($CO_2$-exposed, from drill hole), b) Big Hole (unreacted, from drill hole), and c) I-70 (unreacted, from outcrop). Dry experiments are indicated by dashed circles and open symbols, wet experiments are indicated by solid circles and solid symbols. For the wet experiments, porosity (%) and dolomite content (wt-%) are also indicated.

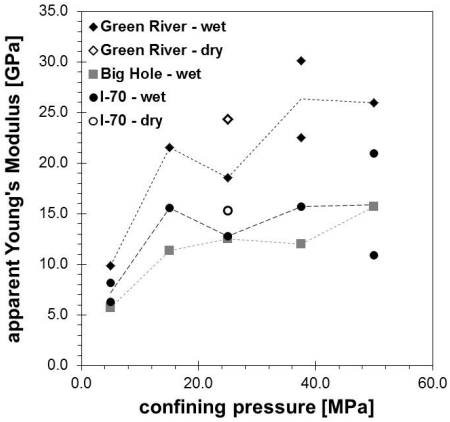


Figure 5. Apparent Young's Modulus vs confining pressure for the Navajo Sandstone obtained from the Green River ($CO_2$-exposed), Big Hole (unreacted) and I-70 (unreacted) sampling locations.

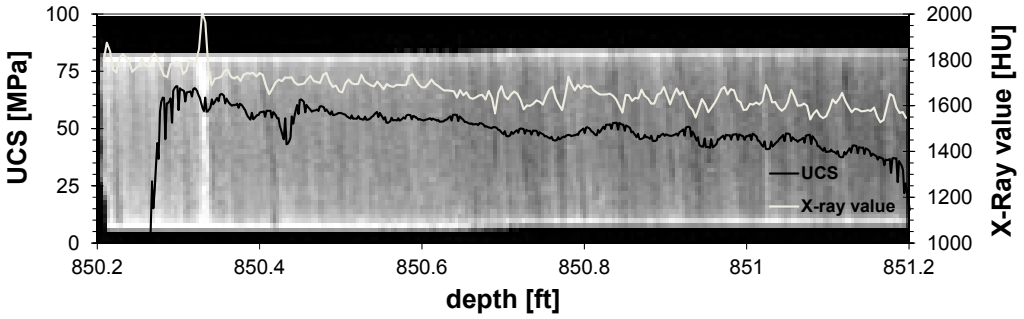


Figure 6. Combined core scratching (UCS – blue line) and CT-scan (X-ray value – red line) plot for a selected section of Navajo Sandstone from the Green River drill core. High X-ray values correspond to light coloured areas on the CT scan, which suggest heavy minerals, such as carbonates (dolomite). As can be seen UCS decreases as carbonate content decreases as well.

## Summary and conclusions

This paper addresses the implications of $CO_2$ migrating up fault from a deep source into shallow reservoirs. We used mineralogical and petrophysical data to study a reaction profile into a tight siltstone layer of the Entrada formation. Reaction patterns were reproduced qualitatively using geochemical modeling. Reactions are considered to be ongoing for at least the past 113 kyears based on U-series dating of travertines from the leaking fault. Within this time period hematite and dolomite dissolution fronts propagated ~10 cm into the layer. Pyrite and ankerite precipitated on and behind the propagating dissolution fronts. A small decrease in porosity between unreacted and reacted intervals is observed suggesting a net destruction of porosity following the reactions.

The impact of $CO_2$ on the mechanical properties of reservoir rock (Navajo sandstone) is also considered to be low and differences to non $CO_2$-reacted samples are rather attributed to burial history/rock heterogeneity than being affected by $CO_2$-water-rock interactions.

Some more detailed work is needed but if these findings are confirmed, then the following conclusions can be drawn: (1) pure diffusion controlled reaction features, involving redox reactions can be qualitatively matched using 1D reactive transport models; (2) at least for the system studied here, such caprock reactions do not lead to a net increase in porosity (and potentially permeability); (3) $CO_2$-water/rock reactions have little or no impact on the strength of quartz-rich sandstones as studied here.

## Acknowledgements

Part of this research is funded by the Dutch Research Program on Carbon Capture and Storage, CATO2. Carbon storage research at Cambridge, Oxford and the British Geological Survey is supported by the UK Department of Energy and Climate Change through the Carbon Capture and Storage research and development programme and Natural Environment Research Council grants NE / F004699 / 1, NE / F002823 / 1 and NEF002645 / 1. Work by G. R. was supported by the U. S. Department of Energy (DOE), Office of Science, Basic Energy Sciences (BES) under Award # ERKCC72. A portion of this Research at Oak Ridge National Laboratory's High Flux Isotope Reactor was sponsored by the U.S. Department of Energy, Office of Basic Energy Sciences.

## References

1. Kampman, N., et al., *Fluid flow and CO2/fluid/mineral interactions during CO2-storage in sedimentary basins.* Chemical Geology, 2014. **369**(0): p. 22-50.
2. Gilfillan, S.M.V., et al., *Solubility trapping in formation water as dominant CO2 sink in natural gas fields.* Nature, 2009. **458**(7238): p. 614-618.
3. Bickle, M.J., *Geological carbon storage.* Nature Geoscience, 2009. **2**(12): p. 815-818.
4. Kampman, N., et al., *Drilling and sampling a natural CO2 reservoir: Implications for fluid flow and CO2-fluid-rock reactions during CO2 migration through the overburden.* Chemical Geology, 2014. **369**(0): p. 51-82.
5. Kampman, N., et al., *Scientific drilling and downhole fluid sampling of a natural CO2 reservoir, Green River, Utah.* Sci. Dril., 2013. **16**: p. 33-43.
6. Kampman, N., et al., *Pulses of carbon dioxide emissions from intracrustal faults following climatic warming.* Nature Geoscience, 2012. **5**(5): p. 352-358.
7. Burnside, N.M., et al., *Man-made versus natural CO2 leakage: A 400 k.y. history of an analogue for engineered geological storage of CO2.* Geology, 2013.
8. Parkhurst, D.L. and C.A.J. Appelo, *User's Guide to PHREEQC (VERSION 2) - a computer program for speciation, batch-reaction, one-dimensional transport, and inverse geochemical calculations.* Water-Resources Investigations Report 99-4259, 1999: p. 326.
9. Wei, L., *Sequential Coupling of Geochemical Reactions With Reservoir Simulations for Waterflood and EOR Studies.* SPE Journal, 2012. **17**: p. 469 - 484.
10. Gasparik, M., et al., *Geological controls on the methane storage capacity in organic-rich shales.* International Journal of Coal Geology, 2014. **123**(0): p. 34-51.
11. Ufer, K., et al., *Quantitative phase analysis of bentonites by the Rietveld method.* Clays and Clay Minerals, 2008. **56**(2): p. 272-282.
12. http://iffwww.iff.kfa-juelich.de/~pipich/dokuwiki/doku.php/qtikws. *SANS data treatment package*. 2014 August 2014].
13. Hinde, A., *PRINSAS - a Windows-based computer program for the processing and interpretation of small-angle scattering data tailored to the analysis of sedimentary rocks.* Journal of Applied Crystallography, 2004. **37**(6): p. 1020-1024.
14. Hangx, S.J.T., et al., *The effects of lateral variations in rock composition and texture on anhydrite caprock integrity of $CO_2$ storage systems.* International Journal of Rock Mechanics and Mining Sciences, 2014. **69**(0): p. 80-92.
15. Hangx, S.J.T., C.J. Spiers, and C.J. Peach, *Mechanical behavior of anhydrite caprock and implications for $CO_2$ sealing capacity.* Journal of Geophysical Research, 2010. **115**(B7): p. B07402.
16. Zoback, M.D. and J.D. Byerlee, *The effect of cyclic differential stress on dilatancy in Westerly granite under uniaxial and triaxial conditions.* Journal of Geophysical Research, 1975. **80**(11): p. 1526-1530.
17. Baud, P., A. Schubnel, and T.-F. Wong, *Dilatancy, compaction, and failure mode in Solnhofen limestone.* Journal of Geophysical Research, 2000. **105**(B8): p. 19289-19303.
18. Wong, T.-f. and P. Baud, *The brittle-ductile transition in porous rock: A review.* Journal of Structural Geology, 2012. **44**(0): p. 25-53.